


Karyopherin Kap114p-mediated trans-repression controls ribosomal gene expression under saline stress

Chung-Chi Liao¹, Sahana Shankar¹, Wen-Chieh Pi², Chih-Chia Chang¹, Golam Rizvee Ahmed¹, Wei-Yi Chen² & Kuo-Chiang Hsia^{1,2,*} 

Abstract

Nuclear accessibility of transcription factors controls gene expression, co-regulated by Ran-dependent nuclear localization and a competitive regulatory network. Here, we reveal that nuclear import factor-facilitated transcriptional repression attenuates ribosome biogenesis under chronic salt stress. Kap114p, one of the karyopherin-βs (Kap-βs) that mediates nuclear import of yeast TATA-binding protein (yTBP), exhibits a yTBP-binding affinity four orders of magnitude greater than its counterparts and suppresses binding of yTBP with DNA. Our crystal structure of Kap114p reveals an extensively negatively charged concave surface, accounting for high-affinity basic-protein binding. KAP114 knockout in yeast leads to a high-salt growth defect, with transcriptomic analyses revealing that Kap114p modulates expression of genes associated with ribosomal biogenesis by suppressing yTBP binding to target promoters, a trans-repression mechanism we attribute to reduced nuclear Ran levels under salinity stress. Our findings reveal that Ran integrates the nuclear transport pathway and transcription regulatory network, allowing yeast to respond to environmental stresses.

Keywords high salinity; karyopherin-β; nucleocytoplasmic transport; TATA-box-binding protein; X-ray crystallography

Subject Categories Chromatin, Transcription, & Genomics; Membrane & Trafficking

DOI 10.15252/embr.201948324 | Received 18 April 2019 | Revised 16 April 2020 | Accepted 30 April 2020 | Published online 2 June 2020

EMBO Reports (2020) 21: e48324

Introduction

Under natural conditions, *Saccharomyces cerevisiae* frequently encounters varying and extreme environments that are far from optimal laboratory settings. Therefore, budding yeast must trigger reprogramming of the transcriptome in response to different

environmental stresses, with the underlying mechanisms that alter gene expression for environmental change adaptation being essential for yeast to survive in nature. Altered genomic expression profiles in budding yeast in response to environmental variations have been documented in the literature [1,2], allowing stress-response genes to be divided into two categories: (i) stress-induced genes (e.g., for heat-shock and antioxidant functions) and (ii) stress-repressed genes (e.g., for translation and ribosome biogenesis). Transcriptional regulation of these stress-response genes allows yeast to redirect resources from cell proliferation to stress resistance. However, the stress-related signaling pathways that affect gene transcription and provide various stress tolerances are not fully understood.

Eukaryotic transcription is catalyzed by three distinct RNA polymerases—RNA polymerase I, II, and III (Pol I, II, and III)—that are all mediated by an essential, evolutionarily conserved TATA-binding protein, TBP [3–5]. In RNA Pol II-mediated transcription, TBP, a component of the transcription initiation factor IID (TFIID) complex, recognizes and binds to the core promoters and initiates assembly of the pre-initiation complex (PIC) by recruiting other general transcription factors (e.g., TFIIA and TFIIB), providing a basal level of transcriptional activity [3,4,6]. Notably, binding of TBP to the core promoters is modulated by several regulatory factors [6], such as TBP-associated factors (TAFs) [7] and human BTA1 (B-TFIID TATA-box-binding protein-associated factor 1) or yeast Mot1 (modifier of transcription 1) [8,9]. In yeast, Mot1 is thought to produce a competitive transcriptional regulation network by forming distinct protein complexes with TBP under conditions of cellular stress, thereby regulating nuclear accessibility of TBP for transcription [10,11]. Additionally, biochemical analyses have also demonstrated that Mot1 inhibits TBP-DNA binding by sequestering TBP from DNA via an ATP-dependent mechanism [12]. Hence, Mot1 modulates transcription through genomic redistribution of TBP from promoters harboring a TATA box to those lacking them [3,13]. Moreover, Mot1 works together with negative cofactor 2 (NC2) to induce dissociation of TBP from TATA-containing promoters, thereby modulating specific gene expression [14,15]. On

¹ Institute of Molecular Biology, Academia Sinica, Taipei, Taiwan

² Institute of Biochemistry and Molecular Biology, College of Life Sciences, National Yang-Ming University, Taipei, Taiwan
 *Corresponding author. Tel: +886-2-2789-9199; E-mail: khsia@gate.sinica.edu.tw

the contrary, TFIIA enhances and stabilizes binding of TBP to TATA box promoters [16–19]. Thus, TFIIA competes with Mot1 and NC2 for TBP binding, restoring the TBP and DNA interaction to induce gene expression [20–22]. Additionally, crystal structure analysis has illustrated that binding of TBP to DNA can also be inhibited by the N-terminal domain of TAF1 (TAF1-TAND) via binding to the concave surface of TBP [23]. Structural comparison of TAF1-TAND and other TAFs (e.g., TAF11 and TAF13) in complex with TBP has further revealed that the TBP-binding domain of these structurally distinct TAFs adopts a highly similar TBP-binding configuration, providing mechanistic evidence of competitive transcriptional regulation by these interacting partners of TBP [24,25].

In eukaryotes, the nuclear envelope (NE) separates nuclear transcription and cytoplasmic translation. Transcription factors (e.g., TBP) synthesized in the cytoplasm need to be imported into the nucleus, whereas the translational machinery (e.g., ribosomal subunits) assembled in the nucleus has to be exported to the cytoplasm. A family of soluble transport factors, termed karyopherin- β (Kap- β) in yeast, facilitates nucleo-cytoplasmic transport. Kap- β s recognize nuclear localization signals (NLS) and nuclear export signals (NES) carried by cargo molecules (either directly or through an adapter, karyopherin- α) to transfer cargoes from one side of the NE-embedded nuclear pore complex (NPC) to the other. Self-dimerization of TBP increases its molecular weight beyond the passive diffusion limit (~40 kDa) of the NPC [26–28]. To facilitate nuclear localization, multiple Kap- β s have been identified that mediate active nuclear import of yeast TBP (γ TBP) (e.g., Kap95p, Kap114p, Kap121p, and Kap123p) [29,30]. Hence, in addition to TAFs, nuclear transport receptors also govern nuclear accessibility of TBP. However, only the interplay between TBP and TAFs involved in transcriptional regulation has been studied extensively. Whether nuclear transport receptors modulate the TBP-mediated gene expression that facilitates environmental change adaptation beyond the nuclear transport function of TBP remains to be elucidated.

Here, we demonstrate that γ TBP binds to Kap114p with an affinity that is four orders of magnitude higher than for other examined Kap- β s (Kap95p and Kap121p). Next, our crystal structure of Kap114p reveals that Kap114p structurally resembles a cargo-bound form of the exportin Cse1p, whereas the highly negative surface charges of Kap114p allow it to bind nucleic acid-binding proteins, such as γ TBP. Biophysical and biochemical analyses together with our crystal structure information reveal two inserts within HEAT repeats (HEAT8 hairpin and HEAT19 loop) of Kap114p bearing protein sequence compositions and secondary structure elements similar to the N-terminal domain of TAF1 (TAF1-TAND) that suppress binding of γ TBP to DNA and transcription factors.

Previously, knockout of *KAP114* in yeast resulted in no detectable growth defects under regular conditions [29]. Hence, we examine whether Kap114p- γ TBP tunes gene expression under different stress conditions. Interestingly, our yeast genetic analyses show that *KAP114* is particularly crucial for yeast to grow under chronic salt stress. Transcriptomic analyses further indicate that, under high-salt conditions, Kap114p attenuates expression of genes involved in ribosomal biogenesis and protein translation pathways by suppressing γ TBP binding to target promoters. We further propose that a reduced level of nuclear Ran under salinity stress may facilitate the Kap114p trans-repression mechanism. Thus, we show how Ran pathway may integrate the nuclear transport pathway and gene

transcription regulatory network through Kap114p, suppressing gene transcription involved in ribosome biogenesis and protein translation and conferring salt tolerance to yeast.

Results

Biochemical characterization of γ TBP and Kap- β interactions

γ TBP localization to the nucleus is facilitated by different Kap- β s, such as Kap95p, Kap114p, and Kap121p [29,30]. To biochemically validate the many interactions that occur between γ TBP and different Kap- β s, we first conducted pull-down assays using purified recombinant proteins. Interestingly, while constitutively active His-tagged RanQ69L pulled down comparable amounts of Kap95p, Kap114p, and Kap121p, pull-down of Kap114p by GST-fused γ TBP (amino acids (aa) 61–240; hereafter γ TBP) was substantially elevated compared to that of Kap95p and Kap121p (Fig 1A and B, Appendix Fig S1A and B), suggesting that γ TBP directly binds Kap114p with a relatively higher binding affinity. Next, we used isothermal titration calorimetry (ITC) to measure dissociation constants (Kds) between γ TBP and Kap- β s. The Kd values of γ TBP and Kap95p or Kap121p were ~10 and 40 μ M, respectively (Fig 1D and E). Notably, under the same experimental conditions, ITC revealed the binding affinity of Kap114p to γ TBP (1 nM) to be four orders of magnitude higher than for Kap95p and Kap121p (Fig 1C), further demonstrating that γ TBP preferably binds Kap114p. Additionally, the respective biphasic ITC-binding profile revealed that multiple binding sites contribute to the interaction between γ TBP and Kap114p (Fig 1C).

The Kap114p crystal structure shows an exportin Cse1p-like fold

To gain structural insights into how Kap114p binds to γ TBP with an affinity in the sub-nanomolar range, we determined the crystal structure of Kap114p. Crystallization of Kap114p in citric acid, bis-tris propane (pH 5.8), PEG3350, EDTA, and ethanol generated hexagonal crystals (space group $P3_12_1$), with one molecule per asymmetric unit. Phase determination was carried out using data collected from seleno-L-methionine-labeled crystals at selenium peak and inflection wavelengths (Appendix Table S1). The final structure was refined to a resolution of 2.5 Å with an *R*-factor of 20.6% (*R*_{free} 25.5%), and there were no outliers in the Ramachandran plot (Appendix Table S1). The overall architecture of Kap114p is comparable to known yeast karyopherin structures (Appendix Fig S1C), and superimposition of Kap114p with the crystal structure of the cargo-bound exportin Cse1p reveals striking structural similarities between their tertiary structures (Fig 1G) [31]: (i) Both Kap114p and Cse1p harbor 20 HEAT repeats that form a right-handed super-helix structure (Fig 1F–H; 19 HEAT repeats in Kap95p); and (ii) two intra-HEAT-repeat inserts found in Kap114p, i.e., the HEAT8 hairpin and the HEAT19 loop, also occur in Cse1p but not in Kap95p (Fig 1F–H, Appendix Fig S1C). As Cse1p forms a nuclear export complex together with its cargo and Ran [31], we next performed a GST pull-down assay to test whether Kap114p simultaneously binds Ran and γ TBP (cargo). In the presence of RanQ69L, pull-down of Kap114p by GST- γ TBP was substantially reduced compared to pull-down in the absence of Ran (Appendix Fig S1D), suggesting the

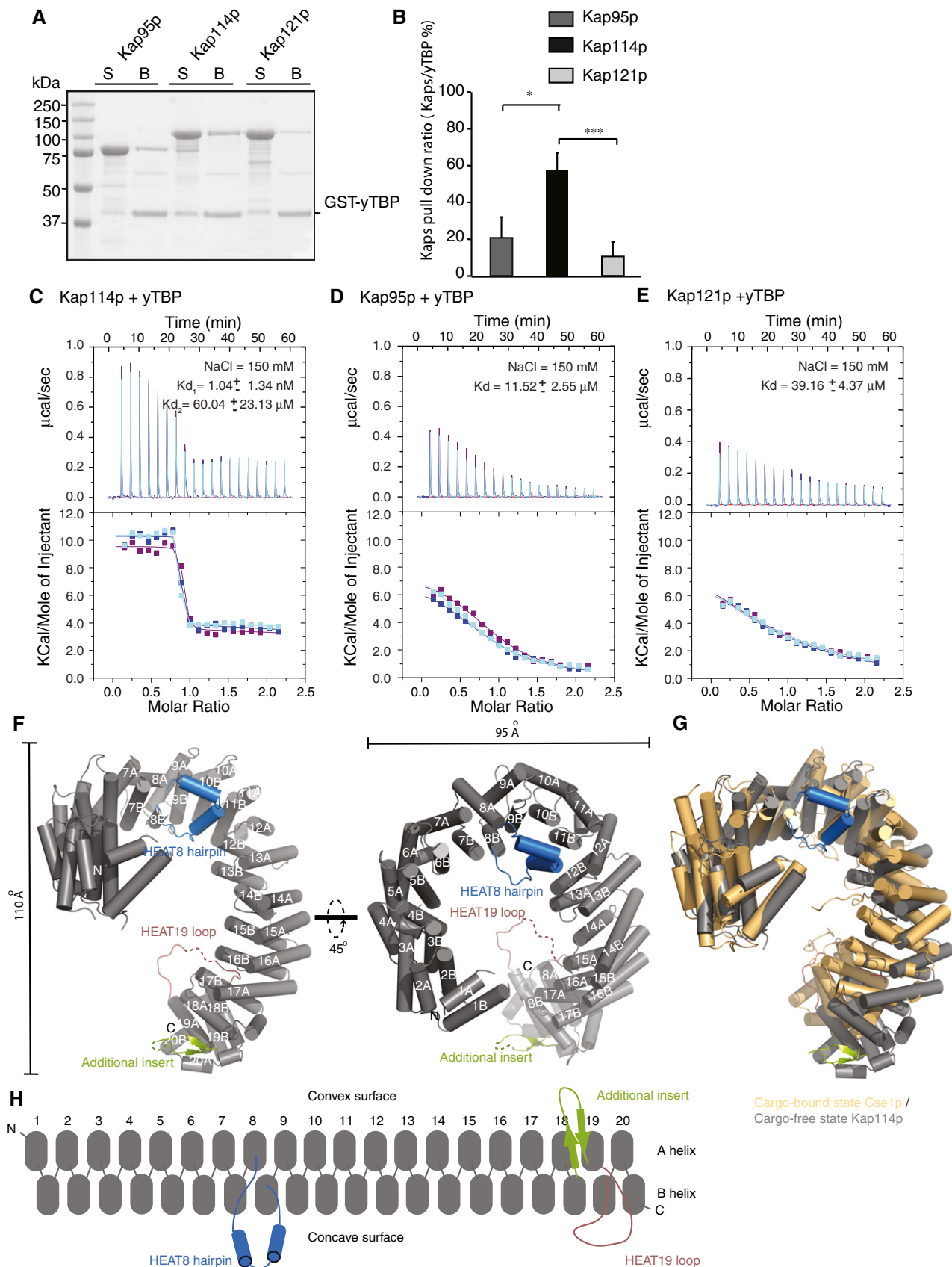


Figure 1.

Figure 1. Biochemical and structural characterization of yTBP and Kap114p interaction.

- A Pull-down assays of yTBP (61–240) with Kap95p, Kap114p, and Kap121p. GST-fused yTBP (61–240) was incubated with recombinant Kap95p, Kap114p, and Kap121p. Unbound (S) and bound (B) samples were analyzed by SDS-PAGE and stained with Coomassie blue.
- B Band intensities of Kap- β s from the SDS-PAGE gels in (A) were quantified and normalized by GST-yTBP intensity. Quantitative plots show percent Kap- β s binding on yTBP.
- C–E ITC titration curves (upper) and binding isotherms (lower) of (C) Kap114p, (D) Kap95p, and (E) Kap121p with yTBP (61–240). Salt concentration and K_d values are indicated.
- F Cartoon representation of the Kap114p crystal structure. The A and B helices composed of each HEAT repeat are shown as gray cylinders. The HEAT8 hairpin, HEAT19 loop, and additional HEAT18/19 loop are highlighted in blue, red, and green, respectively. A 45° rotated view is shown on the right. Overall dimensions of the Kap114p structure are indicated.
- G Superimposition of Kap114p (gray) with cargo-bound Cse1p (light orange; PDB code: 1WAS). The HEAT8 hairpin and HEAT19 loop of Kap114p are colored blue and light green, respectively.
- H Schematic representation of the Kap114p domain configuration using the same color code as shown in (F).

Data information: In (B–E), data represent mean \pm SD from three independent experiments. Differences were assessed statistically by two-tailed Student's *t*-test; **P* < 0.05; ****P* < 0.001.

existence of a mutually exclusive Ran and yTBP-binding site in Kap114p. Thus, although Kap114p (importin) and Cse1p (exportin) show high structural similarity, Kap114p functions as an import receptor.

Cse1p is an exportin dedicated to nuclear export of yeast importin- α (Kap60p; isoelectric point (pI) = 4.8) [32,33], whereas Kap114p imports multiple nucleic acid-binding proteins that bear positively charged surface patches (e.g., yTBP, histone H2A/H2B, and NAP) [29,30,34,35]. Thus, Kap114p and Cse1p should exhibit different surface charge distributions in order to accommodate binding of their cargoes. Electrostatic surface calculations revealed a neutral charge distribution in the concave surface of the Cse1p central region that is crucial for Kap60p binding (Appendix Fig S1E). Interestingly, calculations of electrostatic properties indicated that the concave surface of Kap114p, i.e., where cargoes are supposed to bind, is negatively charged (Appendix Fig S1F and G).

The crystal structure of cargo-free Kap114p showed an open conformation the same as that of the cargo-bound state of Cse1p (Fig 1G). We wondered if this open form of Kap114p can exist in a non-crystalline environment, so we carried out small-angle X-ray scattering (SAXS) analyses to obtain information on its global shape in solution. The $P(r)$ function derived from SAXS data, which reflects the distribution of mean electron density of the molecule, displayed a bimodal distribution with two maxima, implying Kap114p molecule flexibility (Appendix Fig S2A). Furthermore, the profile of the Kap114p Kratky plot is comparable to that of CRM1 (Appendix Fig S2C), an exportin that adopts different conformations in solution [36]. This result suggests that open and closed conformations of Kap114p may co-exist in solution. The theoretical scattering profile generated by our Kap114p model exhibited reasonable agreement with our experimental data (Appendix Fig S2B). Furthermore, we used the *ab initio* modeling method GASBOR for shape determination, which revealed an open ring-like conformation that allowed the crystal structure of cargo-free Kap114p to be docked into the SAXS-derived Kap114p envelope (Appendix Fig S2D and E).

Kap114p interacts with Ran and yTBP with equal stoichiometry

Next, we examined in molecular detail how Kap114p interacts with Ran and yTBP. We biochemically reconstituted Kap114p-RanQ69L and Kap114p-yTBP complexes using recombinant Kap114p,

RanQ69L, and yTBP. Purified Kap114p formed stable complexes with either RanQ69L or yTBP, co-migrating with either one in a sharp mono-dispersed peak in size exclusion chromatography (SEC; Fig 2A and B). The band intensities of Kap114p and Ran on SDS-PAGE suggest a 1:1 equal stoichiometry (Fig 2A), consistent with the ratios found in all Ran-Kap- β complexes [37]. However, since yTBP has been reported to form dimers in solution [26], the stoichiometry of the Kap114p-yTBP complex needed further assessment. Thus, we applied analytic ultracentrifugation with sedimentation velocity (SV-AUC) and sedimentation equilibrium (SE-AUC) to characterize the size distributions of yTBP, Kap114p, and the Kap114p-yTBP complex. SV-AUC revealed that yTBP and Kap114p alone in solution are predominantly a homo-dimer and monomer, respectively, with molecular masses consistent with calculated values (Fig 2C and D). Sedimentation profiles from SV-AUC and SE-AUC of the Kap114p-yTBP complex revealed a molecular mass of ~130 kDa (Fig 2E and F), concordant with the calculated molecular weight of a hetero-dimeric complex, suggesting a 1:1 stoichiometry for the Kap114p-yTBP complex.

Next, we carried out SAXS analysis to determine the global shapes of Kap114p in complex with either RanQ69L or yTBP. The $P(r)$ function derived from SAXS data showed a single peak for both complexes, indicating a single conformation in solution and differing from our assessment of Kap114p alone (Fig 2G and K, Appendix Fig S2A). The bell-shaped Kratky plots of both complexes had maxima of ~1.1 at $q \cdot R_g = \sqrt{3}$, further suggesting a compact folded conformation (Fig 2H and L). Next, we applied GASBOR *ab initio* modeling to generate 10 independent and reproducible models—normalized spatial discrepancy (NSD) = 1.29 ± 0.03 for Kap114p-yTBP and NSD = 1.31 ± 0.06 for Kap114p-RanQ69L—that matched well with our experimental data (Appendix Fig S2F and H). The final SAXS envelopes of both complexes displayed a compact globular shape without a central cavity (Fig 2I and M). These results demonstrate that Ran and yTBP associate with Kap114p, filling the central cavity of the ring-like structure. To dock crystal structures into the SAXS-derived envelopes, we used FoXSDock that predicts interfaces based on experimental data and calculated energies to best fit the SAXS profiles. FoXSDock could place either RanQ69L or yTBP in the center of the horseshoe-shaped Kap114p structure, with the two arms of the horseshoe wrapped around either protein (Fig 2J and N; Appendix Fig S3G and I).

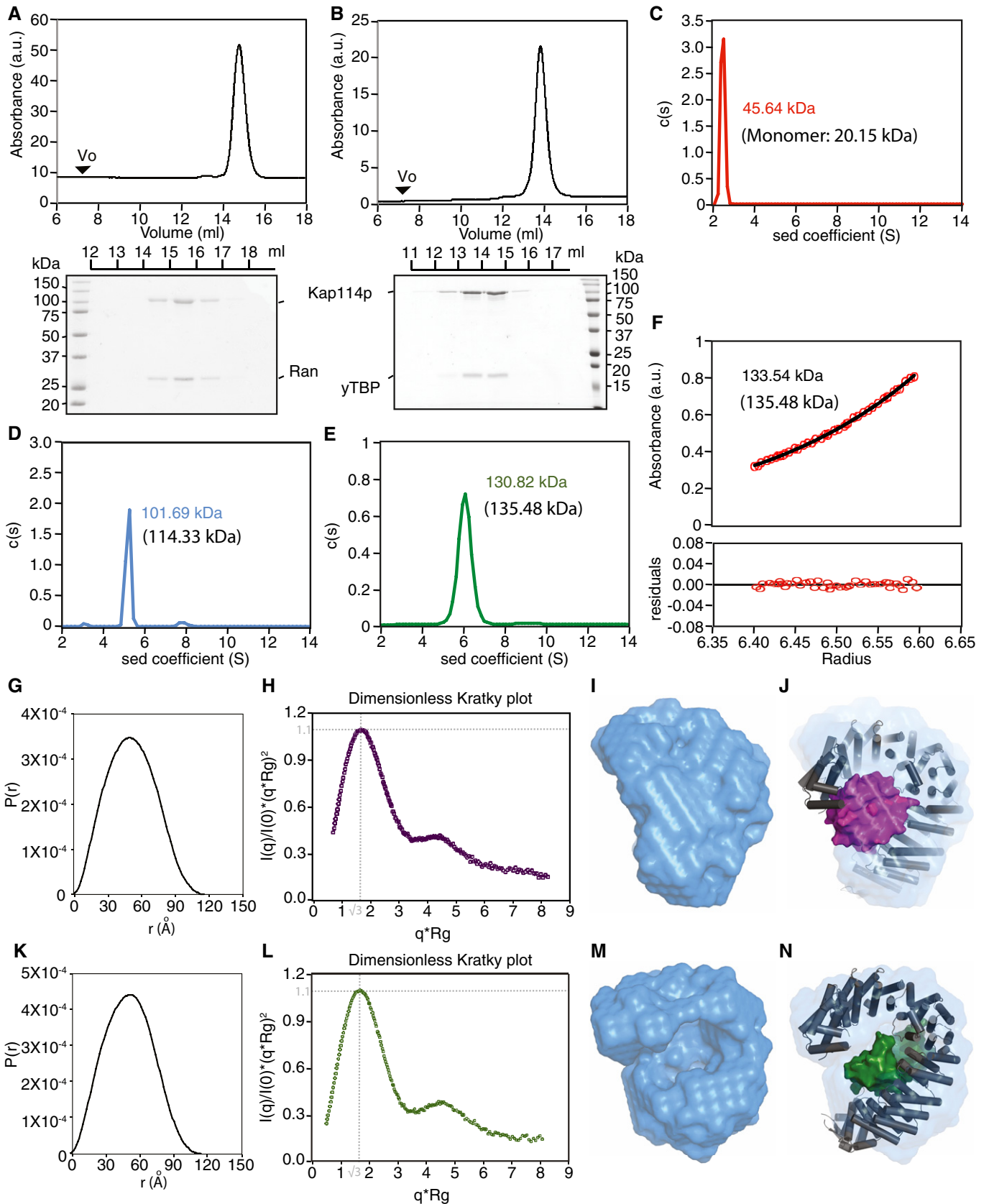


Figure 2.

Figure 2. Ran and yTBP binding by Kap114p.

- A, B Purified recombinant Kap114p was mixed with RanQ69L or yTBP and analyzed by SEC. SEC (Superdex 200) elution profiles of the (A) Kap114p-RanQ69L and (B) Kap114p-yTBP complexes. Peak fractions were analyzed by SDS-PAGE and stained with Coomassie blue. The void volume (V_0) of the peak fraction and absorbance (a.u.) at 280 nm for each complex is indicated.
- C-E SV-AUC analysis of (C) yTBP, (D) Kap114p, and (E) the Kap114p-yTBP complex. The experimental data were analyzed using the Sedfit program and are presented above molecular weights calculated using standards (in brackets).
- F SE-AUC analysis of the Kap114p-yTBP complex. The average molecular mass determined by the Sedfit program was ~133.5 kDa. The lower panel shows the residual difference (SD) between experimental and fitted values.
- G-N Plots of the distance distribution function $P(r)$ for the (G) Kap114p-RanQ69L and (K) Kap114p-yTBP complexes derived from experimental SAXS data using the GNOM program. (H, L) Rg-based dimensionless Kratky plot of the Kap114p-RanQ69L (H) and Kap114p-yTBP (L) complexes. Intersection of the two dotted gray lines indicates features of a compact protein. The *ab initio* envelopes determined by GASBOR for the (I) Kap114p-RanQ69L and (M) Kap114p-yTBP complexes. Models of the (J) Kap114p-RanQ69L and (N) Kap114p-yTBP complexes derived from SAXS profiles using FoXSdock and docked into the *ab initio* envelopes obtained from GASBOR.

The HEAT8 hairpin of Kap114p facilitates Ran binding

Our low-resolution models showed that the HEAT8 hairpin and HEAT19 loop facing the concave surface of Kap114p might physically contact Ran and yTBP. Therefore, we generated two deletion constructs lacking, respectively, the HEAT8 hairpin (aa 347–371, hereafter Kap114p (Δ 347–371)) and the HEAT19 loop (aa 899–956, hereafter Kap114p (Δ 899–956); Fig 3A, Appendix Fig S3C), and then examined their Ran- and yTBP-binding activities.

We biochemically purified Kap114p (Δ 347–371) and Kap114p (Δ 899–956) to homogeneity using multiple steps of a chromatographic approach and further assessed both constructs by SEC, mass spectrometry, and circular dichroism (CD) (Appendix Fig S3D–H). The protein secondary structure composition and solution properties of wild-type Kap114p and the two deletion mutants were comparable (Appendix Fig S3D–H), so they were suitable for further biochemical studies. We then performed biochemical pull-down assays using recombinant proteins to assess whether the HEAT8 hairpin and HEAT19 loop of Kap114p contribute to the binding of Ran and yTBP. Under our pull-down conditions, both of the HEAT8 hairpin and HEAT19 loop deletion mutants retained the ability to interact with GST-yTBP at levels not significantly different to wild-type Kap114p (Fig 3B and C). Furthermore, ITC revealed that the HEAT8 hairpin and HEAT19 loop contribute minimally to the binding affinity of Kap114p and yTBP, as the K_d values between Kap114p (Δ 347–371) or Kap114p (Δ 899–956) and yTBP are ~60 and 30 nM, respectively (Fig 3D and E). Notably, the K_d values of the Kap114p deletion mutants still appeared to be lower than those of other Kap- β s (Fig 1D and E), suggesting that these mutants can still enable transport of yTBP to the nucleus.

Knockout of *KAP114* in yeast cells leads to TBP mislocalization to the cytoplasm [29,30], so we sought to examine whether the HEAT8 hairpin and HEAT19 loop are important for yTBP nuclear transport. To do this, we knocked out *KAP114* in a strain bearing GFP-labeled yTBP (Appendix Fig S5A and C). Under our acquisition conditions, we found that ratios of GFP-yTBP signal between the nucleus and cytoplasm were reduced in the deletion mutant compared to that of wild type (Fig 3F, Appendix Fig S4A), consistent with deletion of *KAP114* leading to mislocalization of yTBP in the cytoplasm. Next, to examine whether *KAP114* mutants can facilitate nuclear transport of yTBP, we expressed wild-type and mutant *KAP114* driven by an endogenous promoter in the *KAP114* knockout strain. Plasmids expressing wild-type or *KAP114* mutants were validated by quantitative RT-PCR, showing 1.5- to 2-fold expression

enhancement relative to that of the chromosomal *KAP114* gene (Appendix Fig S4B). Western blot analyses further revealed that protein levels of plasmid expressing FLAG-tagged wild-type or *KAP114* mutants were comparable (Appendix Fig S4E and G). Cytoplasmic yTBP mislocalization due to *KAP114* knockout could be rescued by our wild-type and deletion mutants (Fig 3F, Appendix Fig S4A), corroborating that these *KAP114* mutants are still able to deliver yTBP to the nucleus. These results imply that the HEAT8 hairpin and HEAT19 loop of Kap114p are not crucial for nuclear transport of yTBP.

Notably, pull-down of Kap114p (Δ 347–371) by His-Ran Q69L was substantially diminished compared to that of wild-type and the Kap114p (Δ 899–956) mutant (Fig 3G and H), suggesting that the HEAT8 hairpin is crucial for Ran binding, as is the case for importin- β [38,39]. Furthermore, in a GST pull-down assay with a 1:4:8 mix ratio of Kap114p:yTBP:RanQ69L, wild-type Kap114p and Kap114p (Δ 347–371) showed comparable SDS-PAGE band intensities in the protein-bound fractions to assays in the absence of Ran Q69L (Fig 3I and J), consistent with the fact that they have comparable binding affinities to yTBP. As expected, pull-down of wild-type Kap114p by GST-yTBP was significantly different in the presence or absence of Ran Q69L (Fig 3I and J). However, the amounts of Kap114p (Δ 347–371) pulled down by GST-yTBP displayed minimal differences regardless of the presence or absence of Ran Q69L (Fig 3I and J). Taken together, these results suggest that HEAT8 hairpin-mediated binding of Ran partially dissociates yTBP binding.

Kap114p suppresses complex formation of yTBP, DNA, and TFIIA

Kap114p shows a high affinity for yTBP and prevents yTBP homodimerization. Moreover, while the HEAT8 hairpin and HEAT19 loop of Kap114p do not play an important role in nuclear import of yTBP, we found that their protein sequences are similar to the N-terminal domain of TAF1 (TAF1-TAND). TAF1-TAND, which is composed of TAND1 and TAND2 units, modulates interaction of yTBP with TATA box DNA and transcription factors (e.g., TFIIA) [22,40]. A set of TAND1 residues structurally mimics nucleobases and the sugar-phosphate backbone of DNA and can thereby mediate interactions between the two α -helices of TAND1 and the concave surface of yTBP. Remarkably, these residues are also well preserved in the HEAT8 hairpin of Kap114p, as well as its homologs across species (Fig 4A, Appendix Fig S3A) [24]. Additionally, the HEAT19 loop of Kap114p is highly negatively charged, presenting protein sequence properties similar to those of TAND2, which is a conserved

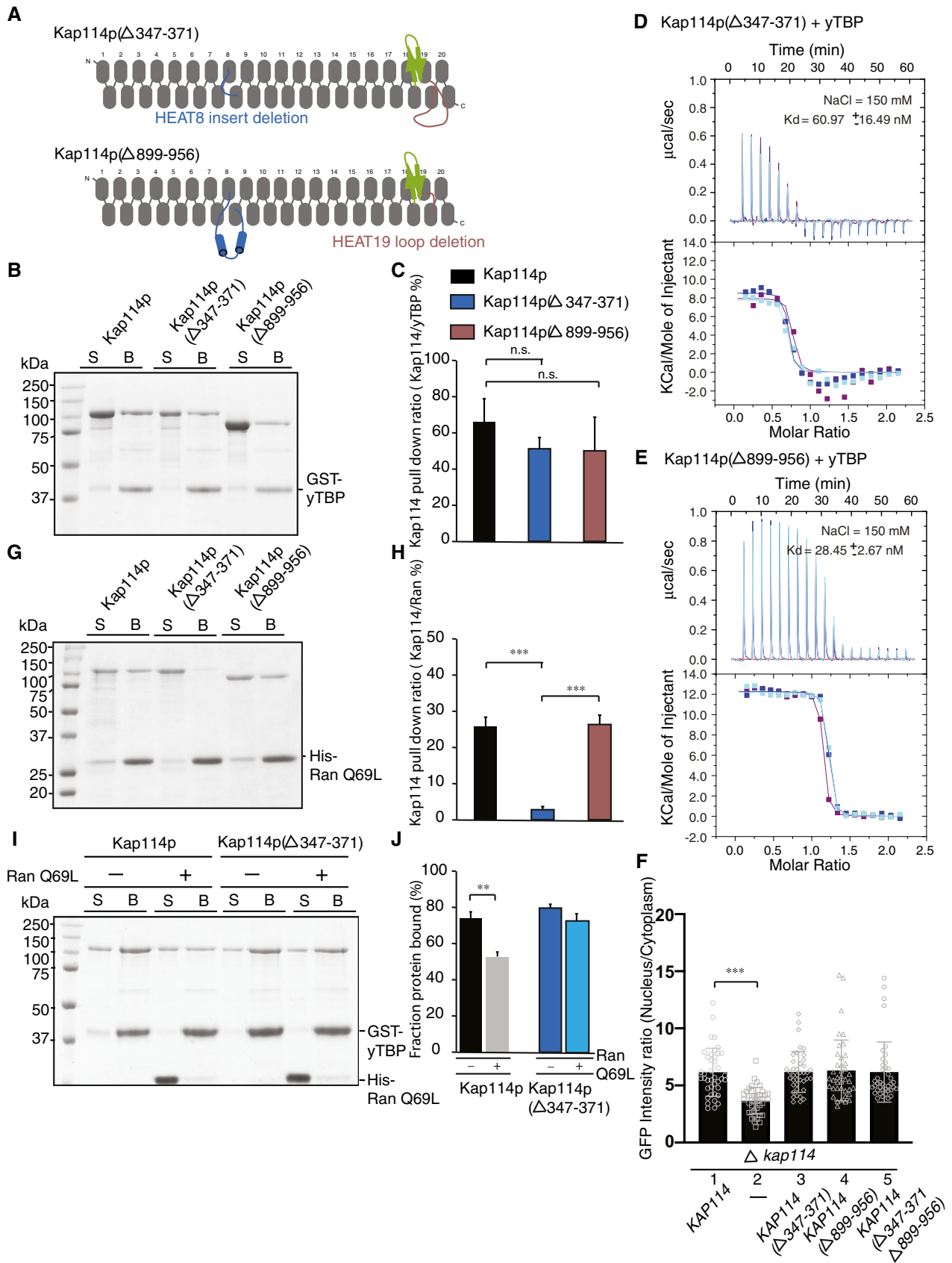


Figure 3.

Figure 3. The HEAT8 hairpin of Kap114p is crucial for Ran binding.

- A Schematic representation of the domain structures of the two deletion mutants, Kap114p ($\Delta 347\text{--}371$) and Kap114p ($\Delta 899\text{--}956$).
- B Pull-down assays of yTBP with Kap114p, Kap114p ($\Delta 347\text{--}371$), and Kap114p ($\Delta 899\text{--}956$). GST-fused yTBP (61–240) was incubated with recombinant Kap114p, Kap114p ($\Delta 347\text{--}371$), and Kap114p ($\Delta 899\text{--}956$). Unbound (S) and bound (B) samples were analyzed by SDS–PAGE and stained with Coomassie blue.
- C Band intensities of Kap- β s from the SDS–PAGE gels in (B) were quantified and normalized by GST–yTBP intensity. Quantitative plots show percent Kap- β s binding on yTBP.
- D, E ITC titration curves (upper) and binding isotherms (lower) of (D) Kap114p ($\Delta 347\text{--}371$) and (E) Kap114p ($\Delta 899\text{--}956$) with yTBP (61–240). Salt concentration and K_d values are indicated.
- F Relative fluorescence GFP intensities in the nucleus and cytoplasm of wild type, *KAP114* knockout strains, and *KAP114* knockout strains rescued by *KAP114* deletion mutants.
- G His-tagged RanQ69L was incubated with recombinant Kap114p, Kap114p ($\Delta 347\text{--}371$), and Kap114p ($\Delta 899\text{--}956$). Unbound (S) and bound (B) samples were analyzed by SDS–PAGE and stained with Coomassie blue.
- H Band intensities of Kap- β s from the SDS–PAGE gels in (G) were quantified and normalized by His–Ran intensity. Quantitative plots show percent Kap- β s binding on His–Ran.
- I GST pull-down assays of yTBP (61–240) with Kap114p or Kap114p ($\Delta 347\text{--}371$) in the presence or absence of RanQ69L. GST-fused yTBP (61–240) was incubated with recombinant Kap114p and His-tagged RanQ69L at a molar ratio of 1:4:8 Kap114p:yTBP:RanQ69L. Unbound (S) and bound (B) samples were analyzed by SDS–PAGE and stained with Coomassie blue.
- J Analysis of Kap114p dissociation from yTBP in the presence of RanQ69L. Band intensities of Kap114p and Kap114p ($\Delta 347\text{--}371$) from the SDS–PAGE gels were used to determine the average fraction of bound protein.

Data information: In (C–E, H and J), data represent mean \pm SD from three independent experiments. In (F), data represent mean \pm SD from four independent experiments (40 yeast cells in total for each strain; 10 cells for one experiment). Differences were assessed statistically by two-tailed Student's *t*-test; n.s.: not significant; ***P* < 0.01; ****P* < 0.001.

regulatory yTBP-binding motif also identified in higher eukaryotes (Fig 4A, Appendix Fig S3B) [24].

The HEAT8 hairpin and HEAT19 loop are separated by more than 500 residues, i.e., vastly different to the 10 residues separating TAND1 and TAND2. Next, we used electrophoretic mobility shift assay (EMSA) to determine whether Kap114p could regulate the activity of yTBP in a way similar to TAF1, i.e., by modulating the interaction of TBP and DNA. Under our experimental conditions, yTBP was able to bind the FAM (Fluorescein amidite) 5'-labeled TATA-box double-stranded DNA in a concentration-dependent manner, leading to band shift to a higher position on the gel (Fig 4B). Interestingly, the shifted bands induced by yTBP disappeared when Kap114p was applied in a dose-dependent manner (Fig 4C), suggesting that Kap114p prevents interaction of yTBP and DNA.

Furthermore, we carried out super-shift EMSA using recombinant TFIIA to examine whether Kap114p blocks yTBP and TFIIA interaction [17,41]. Under our experimental conditions, TFIIA induced multiple super-shift bands on the gel in a dose-dependent manner in the presence of yTBP (Fig 4D), consistent with TFIIA being able to stabilize yTBP and DNA interaction to form a higher-order complex structure. Moreover, the intensities of the super-shifted bands that represent the complex were dramatically reduced when we applied increasing concentrations of wild-type Kap114p to the reaction (Fig 4E), indicating suppression of ternary complex formation by Kap114p. Taken together, our analyses indicate that Kap114p is able to suppress interaction between TBP and DNA as well as other transcription factors.

KAP114 is crucial for yeast to grow in high-salt conditions

We then applied yeast genetic approaches to examine in a cellular context our biochemical findings of TAF1-TAND-like motifs in Kap114p. To do this, we generated yeast strains in which *KAP114* was knocked out (Appendix Fig S5A and B). Single knockout of *KAP114* in yeast did not result in detectable growth defects in the regular media (Appendix Fig S5D). Next, to examine whether

Kap114p is involved in regulating stress-responsive gene expression, we grew *KAP114* knockout and wild-type strains under different stress conditions. Interestingly, whereas *KAP114* knockout and wild-type strains displayed comparable growth rates under regular and many stress conditions (Appendix Fig S5D and E), the *KAP114* knockout strain grew much more slowly in high-salt conditions compared to the wild-type strain (Fig 5A).

Furthermore, yeast spot-based assays showed that the expression of wild-type *KAP114* with or without FLAG tags (driven by an endogenous promoter) rescued the high-salt growth defect of the *KAP114* knockout strain, even though RT–qPCR revealed slightly reduced *KAP114* transcript levels from wild-type-expressing plasmid (~ 30% reduction relative to chromosomal *KAP114* gene) under high-salt conditions (Fig 5B, Appendix Fig S4C and D). However, whereas the HEAT8 hairpin and HEAT19 loop deletion mutants presented slightly increased or comparable protein levels relative to wild type (Appendix Fig S4E and G), they did not exhibit the same effect (Fig 5B, lane 4 and 5, Appendix Fig S4D, F, and H). We found that: (i) the HEAT8 hairpin and HEAT19 loop of Kap114p do not play a crucial role in nuclear transport of yTBP (Fig 3F); (ii) Kap114p suppresses the yTBP and DNA interaction (Fig 4C); and (iii) the HEAT8 hairpin and HEAT19 loop mutants cannot rescue the yeast growth defects of *KAP114* knockout under high-salt conditions (Fig 5B). Therefore, next, we examined whether Kap114p regulates yTBP-mediated transcription beyond its nuclear transport function.

The Kap114–yTBP pathway modulates gene expression under chronic salinity stress

To identify potential genes affected by *KAP114* knockout, we carried out next-generation sequencing to analyze the transcriptomic profiles of wild-type and *KAP114* knockout strains under high-salt conditions (1.5 M NaCl), and we present the results as a heatmap (Fig 5C; triplicate samples, *P* < 0.05, TPM of control > 10, [fold change] > 1.5). We identified 641 up- and 415 down-regulated genes with > 2-fold change, which were further assessed by gene ontology (GO) enrichment analysis to establish specific annotations. Notably,

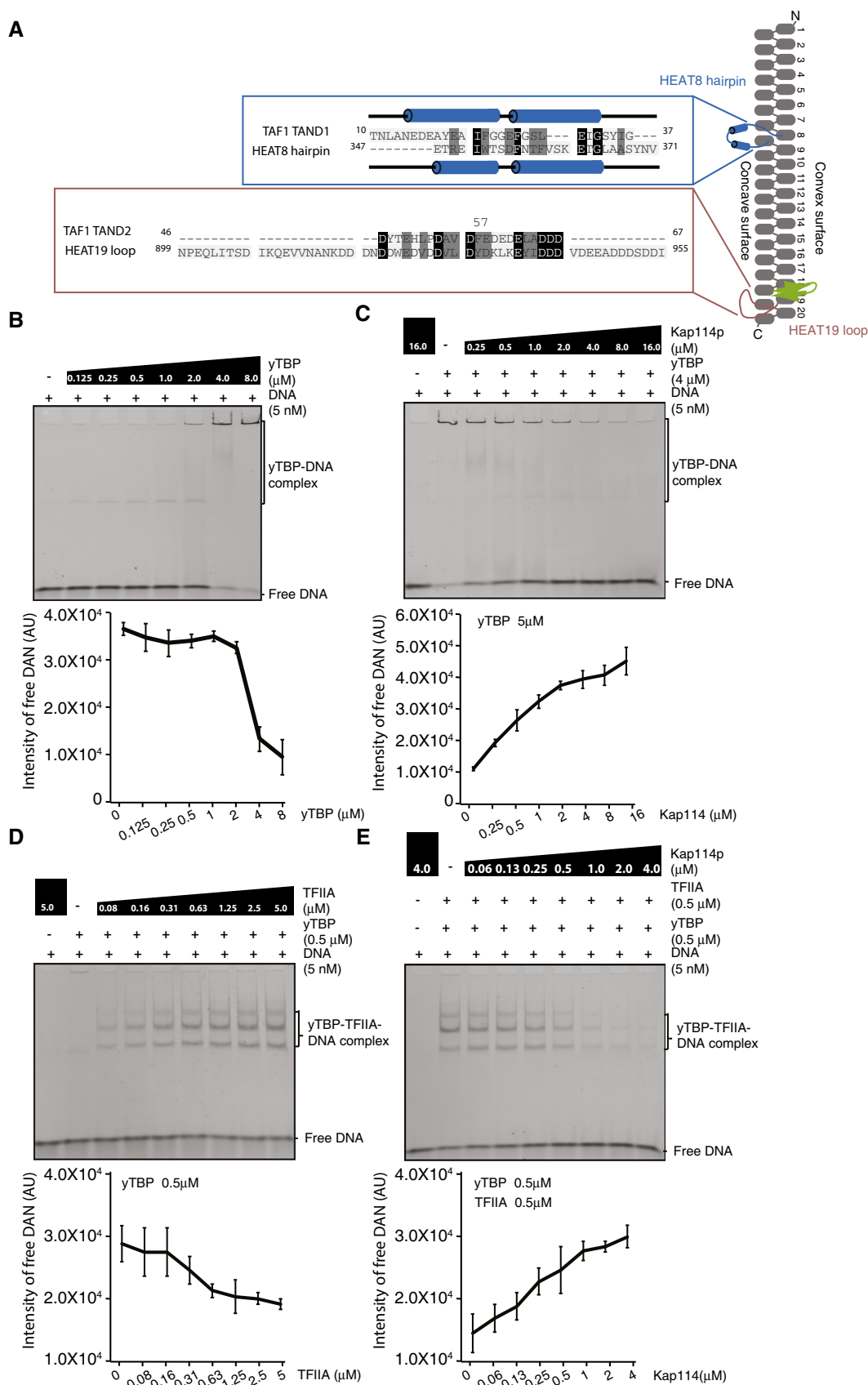


Figure 4.

Figure 4. Kap114p modulates interaction between yTBP and DNA/TFIIA.

- A Protein sequence alignment of the HEAT8 hairpin and TAF1-TAND1, and the HEAT19 loop and TAF1-TAND2 (numbers represent amino acid positions). α -helices were assigned based on crystal structures and are depicted as blue cylinders. The Phe57 anchor residue of TAND2 is indicated [24]. Black color highlights amino acid identity, and gray shading indicates amino acids with similar properties.
- B EMSA analysis of yTBP binding to DNA. We incubated 5 nM FAM-labeled oligonucleotide (TGTATGTATATAAAAC) with indicated concentrations of purified yTBP (0.125–8 μ M) and then analyzed binding by 6% non-denaturing PAGE. Band intensities of free DNA from the gels (Top panel) were quantified and plotted (Bottom panel).
- C Indicated concentrations (0.25–16 μ M) of purified recombinant Kap114p were incubated with yTBP (4 μ M) and FAM-labeled DNA (5 nM), followed by native PAGE analysis. Kap114p (16 μ M) was incubated with DNA without yTBP as a control. Band intensities of free DNA from the gels (Top panel) were quantified and plotted (Bottom panel).
- D Super-shift EMSA analysis of TFIIA binding to yTBP-DNA complex. We incubated 5 nM FAM-labeled DNA and yTBP (0.5 μ M) with indicated concentrations of purified TFIIA (0.08–5 μ M) and then analyzed binding by 6% non-denaturing PAGE. Band intensities of free DNA from the gels (Top panel) were quantified and plotted (Bottom panel).
- E Indicated concentrations (0.06–4 μ M) of purified Kap114p were added to the reaction containing 0.5 μ M of TFIIA, yTBP, and FAM-labeled DNA (TGTATGTATATAAAAC), before conducting native PAGE analysis. TFIIA and Kap114p (4 μ M) were incubated with DNA without yTBP as a control. Band intensities of free DNA from the gels (Top panel) were quantified and plotted (Bottom panel). Electrophoretic bands containing protein–DNA complex and free DNA are indicated.

Data information: In (B–E), data represent mean \pm SD from three independent experiments.

our GO analysis revealed that up-regulated genes are substantially enriched for processes associated with ribosome biogenesis and assembly (Fig 5D; $P < 0.05$, TPM of control > 10 , |fold change| > 2). Repression of ribosomal protein genes, as well as genes involved in protein synthesis, has been observed during different stress responses, including for high salinity [1,2]. Our observation of up-regulated gene expression related to ribosome biogenesis and assembly in the *KAP114* knockout strain could reflect an imbalance in protein synthesis, leading to the high-salt growth defect.

Next, we examined by RT-qPCR four genes encoding ribosomal subunits (*RPS22A*, *RPL30*, *RPS17B*, and *RPL14A*), one gene encoding an elongation factor (*TEF4*), two genes encoding tRNA synthetase (*KRS1* and *FRS1*), one gene encoding a translation initiation factor (*TIF1*), and one gene encoding a translation inhibitor (*ASC1*) for their mRNA levels under regular and high-salt conditions. Under regular conditions, the fold change in gene expression of most of these selected genes (except for *KRS1*, for which transcript was repressed) was comparable between wild-type and *KAP114* knockout strains (Fig 5E). Moreover, in wild-type yeast, the expressions of most of these selected genes (except for *TIF1*) were indeed suppressed under long-term salt stress compared to under regular conditions (Appendix Fig S5F). In contrast, in the *KAP114* knockout strain, the fold change in gene expression of most of the selected genes was significantly elevated, no matter whether we compared the outcomes with those of the wild type under high-salt conditions or the knockout mutant under regular conditions (Fig 5F; Appendix Fig S5G). Since our EMSA analyses demonstrated that Kap114p inhibits TBP and DNA interaction, we hypothesize that Kap114p enables repression of the expression of genes involved in ribosome biogenesis and protein synthesis under long-term high-salt conditions.

Furthermore, we sought to examine whether Kap114p-mediated gene repression operates by modulating yTBP binding at gene promoters. Hence, we examined yeast strains (wild type and *KAP114* knockout) bearing yTBP-GFP by chromatin immunoprecipitation-quantitative PCR (ChIP-qPCR) using anti-GFP antibody. Our ChIP-qPCR analyses showed a 2- to 3-fold increase in DNA quantity of selected genes (except for *CLB2*) in the *KAP114* knockout strain compared to wild type under high-salt conditions (Fig 5G). *CLB2* encodes a cyclin that controls the cell cycle at the G2/M transition [42], and it served here as a negative control. These results may indicate that under high-salt treatment: (i) Occupancy of yTBP at the promoter of selected genes in the *KAP114* knockout strain was

enhanced; or (ii) binding of yTBP at the promoter of selected genes in the wild type was repressed. Next, we separately plotted our wild-type and mutant ChIP-qPCR results and found that, under high-salt conditions, binding of yTBP at the promoter of these genes in the wild type was suppressed (Appendix Fig S5H). However, the reduction in yTBP binding could be restored in the *KAP114* knockout strain (Appendix Fig S5I). These results suggest that, under salinity stress, Kap114p suppresses binding of yTBP to the promoter of genes related to ribosome biogenesis and protein synthesis.

RanGTP causes dissociation of the cargo•transport factor complex by binding to transport factors (Appendix Fig S1D). Under cellular stresses such as UV irradiation or heat shock, the amount of Ran in the nucleus declines [43]. Therefore, we sought to examine whether nuclear Ran levels also decrease under chronic high-salt treatment, diminishing free nuclear Ran and thereby preventing yTBP and DNA interaction in the nucleus. Our Western blot analysis shows that the amount of yTBP-GFP in nuclear fractions isolated from regular conditions was comparable to that under high-salt conditions (Fig 5H and I). Interestingly, under our high-salt conditions, nuclear Ran was much reduced relative to under regular conditions (Fig 5H and J), similar to observations reported for other stress conditions [43]. These results lead us to propose that, under high-salt conditions, disruption of the Ran gradient could decrease liberation of yTBP from Kap114p in the nucleus, attenuating gene expression in response to salt stress.

Discussion

Gene duplication and functional divergence have been proposed as important evolutionary mechanisms driving expansion of the Karyopherin- β protein family in order to endow it with the diverse functions that it carries out [44]. Multiple lines of evidence suggest that a paralogous gene pair, probably created by gene duplication, encodes Kap114p and Cse1p. First, among Kap- β s, Kap114p has been shown to be the most similar to Cse1p at the level of primary protein sequence (18% identity and 43% similarity) [29]. Second, our crystal structure of Kap114p further revealed high structural similarity to Cse1p, including two HEAT repeated inserts (HEAT8 hairpin and HEAT19 loop). Third, both the *KAP114* and *CSE1* genes are located on chromosome VII and are separated by only ~4,000 nucleotides. Functional divergence may occur after gene duplication, resulting in

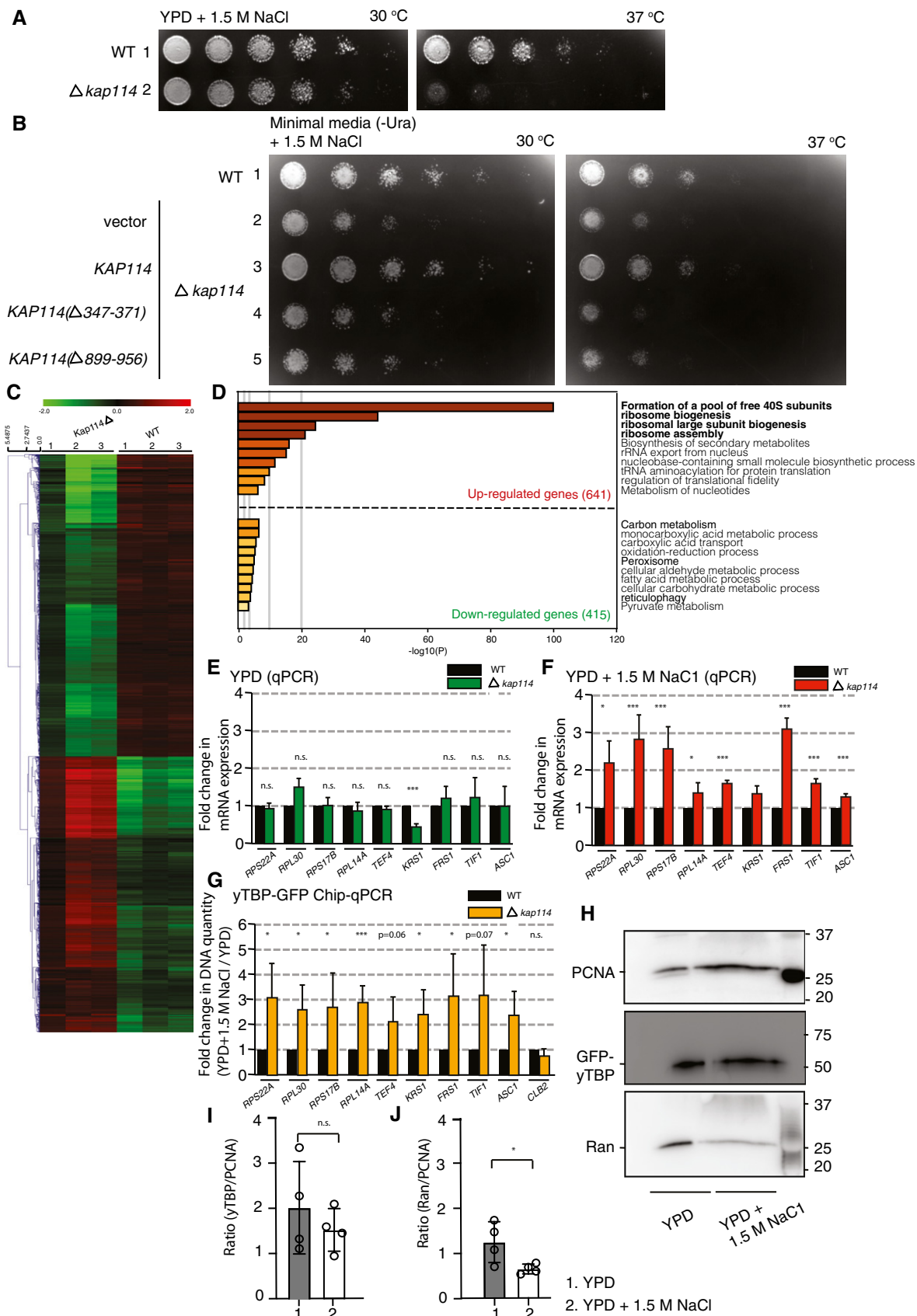


Figure 5.

Figure 5. Kap114p suppresses gene expression under salt stress.

- A Wild-type and *KAP114* knockout strains were diluted serially and spotted onto YPD plates in the presence of 1.5 M NaCl.
- B The *KAP114* knockout strain was transformed with vector control (lane 2) and a plasmid containing wild-type *KAP114*, *KAP114* ($\Delta 347$ – 371), or *KAP114* ($\Delta 899$ – 956) (lanes 3–5). Wild-type and *KAP114* knockout strains containing plasmids were serially diluted and grown in minimal medium plates supplemented with 1.5 M NaCl. Growth temperatures are indicated.
- C A heatmap generated by three independent biological replicates shows gene expression profiles of wild-type and *KAP114* knockout strains grown in the presence of 1.5 M NaCl. The Log_2 (fold change) values and the color scale are shown.
- D Gene ontology enrichment analysis of up- and down-regulated genes, analyzed separately using Metascape (<http://metascape.org>). The top 10 significant GO terms (biological pathways and processes) associated with up- and down-regulated genes are shown. The y-axis represents the GO category (ribosomal biogenesis pathways/processes are highlighted in bold), and the x-axis represents the $-\text{Log}_{10}$ (*P*-value) of GO terms.
- E, F (E) qPCR analysis of gene expression in the *KAP114* knockout strains (green bars) compared to wild type (black bars) under regular conditions. (F) qPCR analysis of gene expression in the *KAP114* knockout strain (green bars) compared to wild type (black bars) grown in high-salt conditions. qPCR fold changes in mRNA expression are relative to control (YPD media, black bars). Actin was used as the internal control.
- G ChIP-qPCR assays showing yTBP-GFP binding to the promoter of indicated genes in wild-type and *KAP114* knockout strains grown in high-salt conditions (light green bars) compared to under regular conditions (black bars). Chip-qPCR fold-enrichment is relative to control (YPD media, black bars).
- H Endogenous Ran, GFP-yTBP, and proliferating cell nuclear antigen (PCNA; loading control) in nuclear fractions isolated from wild-type yeast grown in regular and high-salt conditions were analyzed by Western blot using antibodies for Ran, GFP, and PCNA.
- I, J Analysis of Ran and GFP-yTBP in nuclear fractions isolated from wild-type yeast grown in regular and high-salt conditions. The combined bar and scatter plot shows the band intensity ratios of Ran (I) and GFP-yTBP (J) over PCNA. Each dot represents an individual data point.

Data information: In (E), data represent mean \pm SD, *N* = 5. In (F, G), data represent mean \pm SD, *N* = 3. In (I, J), data represent mean \pm SD from four independent experiments. Differences were assessed statistically by two-tailed Student's *t*-test; **P* < 0.05; ***P* < 0.01; ****P* < 0.001; n.s.: not significant.

a common backbone with largely different electrostatic potentials on the concave surface, as well as different properties of hosted intra-HEAT repeat inserts, both of which are important for accommodating the nuclear import of highly basic proteins.

TAF1 interacts with yTBP via its TAND component comprising TAND1 and TAND2 to modulate gene transcription. Hydrophobic residues on two α -helices of TAND1 that mimic base or ribose moieties of DNA facilitate DNA interaction [24]. Negatively charged residues of TAND2, together with an aromatic amino acid, interact with highly basic yTBP [24]. TAND2 represents a conserved and aspartic acid/glutamic acid-rich TBP-binding motif that has been identified in many structurally distinct proteins such as TFIIA, Brf1, and Mot1 [45]. Notably, the HEAT8 hairpin and HEAT19 loop of Kap114p display protein sequence compositions and secondary structure elements similar to TAND1 and TAND2, respectively. Importantly, these protein properties are conserved across species. Our biochemical analyses further reveal that the HEAT8 hairpin and HEAT19 loop play a crucial role in suppressing interactions between yTBP and DNA as well as other transcription factors. These two intra-HEAT repeat inserts are ~500 residues apart, making it difficult for them to be identified by traditional bioinformatics approaches. However, our structural and biochemical results suggest that the three-dimensional arrangement of Kap114p allows these two HEAT-repeat inserts to operate in concert, thereby conducting roles comparable to those performed by TAF1-TAND.

Ribosome abundance controls the rate of protein synthesis. Hence, ribosome biosynthesis needs to be coordinately regulated and it is essential for cell growth and proliferation. The TOR signaling pathway elevates ribosomal protein gene transcription via multiple transcriptional factors (e.g., Rap1p [46] and Fhl1p [47]). However, down-regulation of ribosomal protein genes under many stress conditions suggests that additional mechanisms mediated by repressors are involved [48]. CRF1p has been identified as a transcriptional repressor that inhibits transcription of ribosomal protein genes by trans-localizing to the nucleus when the rapamycin (TOR) signaling pathway is blocked [49]. Here, we show that, in the

Kap114p-yTBP-facilitated transcription repression pathway, Kap114p represses binding of yTBP to the promoter region of target genes (e.g., ribosomal protein genes) instead of changing the nuclear localization of yTBP, thereby down-regulating ribosomal biogenesis and protein translation under salt stress (Fig 6). The trans-repressive activity identified here for Kap114p has also been reported for many nuclear receptors that interfere with gene expression through protein–protein interactions with transcription factors [50].

As it does with other Kap- β s, RanGTP disassembles Kap114p-yTBP complexes. Thus, due to the greater binding affinity between Kap114p and yTBP, a reduction in nuclear Ran levels under high-salt conditions could lead to a decrease in free yTBP in the nucleus, diminishing the TAF-mediated interaction of yTBP with gene promoters. Additional mechanisms that unload yTBP in the nucleus may also be involved. For instance, post-translational modification by sumoylation of Kap114p residue 909 has been proposed to release cargoes from Kap114p [51]. Lysine residue 909 lies within the unstructured HEAT19 loop according to our Kap114p crystal structure. Moreover, we cannot exclude the possibility that regulation of gene expression allowing yeast to survive under high-salt stress could be a combinatorial effect of the repressive activities of multiple Kap114p-delivered cargoes (e.g., Nap1p, H2A, and H2B) [52,53]. However, we propose a general mechanism by which the nuclear transport factor Kap114p trans-represses the activity of cargoes and controls gene expression. Importantly, we show through Kap114p how Ran pathway may coordinate the nuclear transport pathway and the gene transcriptional regulatory network to respond to environmental stresses.

Materials and Methods

Protein expression and purification

Yeast (*S. cerevisiae*) full-length Kap95p, Kap114p, and Kap121p were amplified by PCR and inserted into the pGEX6p1 expression vector (GE Healthcare) that contains a PreScission cleavage site.

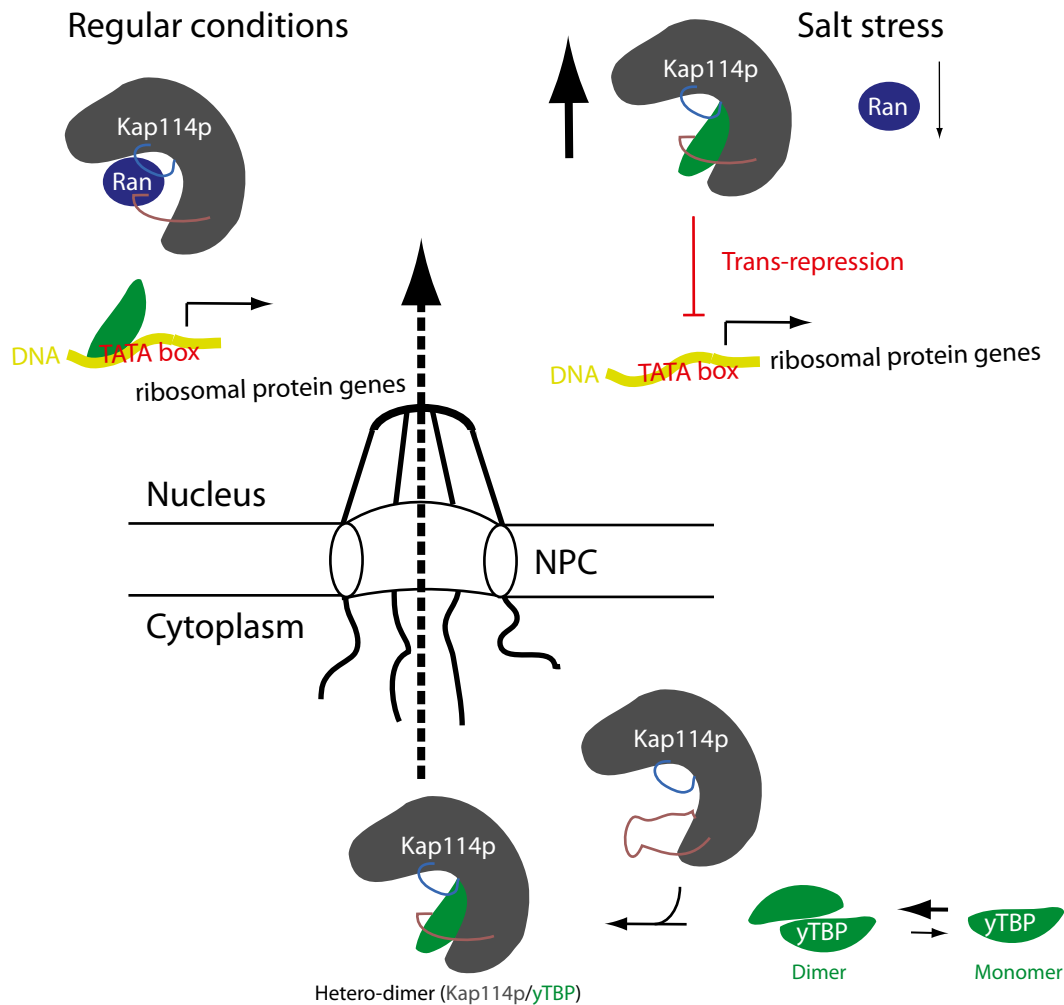


Figure 6. Schematic model of how Kap114p mediates trans-repression of gene expression.

Schematic representation of how Kap114p regulates gene expression. Under normal growth conditions, RanGTP liberates yTBP from Kap114p, allowing gene expression. As nuclear Ran levels are reduced under salt stress, binding of Kap114 to yTBP is enhanced, thereby trans-repressing yTBP activity and down-regulating gene expression.

Proteins were expressed using the *Escherichia coli* Rosetta strain (Novagen). Cell culture was induced by overnight incubation with 0.5 mM IPTG at 18°C. Cells were harvested and resuspended in lysis buffer [20 mM HEPES (pH 7.4), 150 mM NaCl, 3 mM DTT]. The cells were lysed by French press, and the lysate was centrifuged for 30 min at 15,000 g. The supernatant was incubated with GST resins (GE Healthcare), and the GST-fused protein was then eluted by a buffer containing 50 mM of reduced glutathione. The GST-tag was removed by PreScission protease before protein samples were further purified through HiTrap Q HP columns and SEC (Superdex 200 16/60). Protein quality was analyzed and confirmed by SDS-PAGE. Deletion mutants of Kap114p were expressed and purified using an identical protocol.

Yeast (*S. cerevisiae*) yTBP (61–240) was cloned into a modified pET28a vector with a PreScission cleavage site at the N-terminus. The same bacterial strain and protein overexpression strategy used to express Kap proteins were applied to express His-yTBP. Cells were harvested and suspended in phosphate buffer containing 150 mM NaCl and 3 mM β -mercaptoethanol. After cell lysis, the

lysate was clarified by centrifugation and the supernatant was incubated with Ni beads (Qiagen) for 30 min, followed by a prewash with 25 mM imidazole. Proteins were eluted with buffer containing 250 mM imidazole, and the fractions were pooled and dialyzed against buffer [20 mM HEPES (pH 7.4), 150 mM NaCl, 3 mM DTT] overnight. After dialysis, protein samples were loaded into HiTrap SP HP columns and eluted by a salt gradient. Protein samples were then further purified by SEC (Superdex 200 16/60) and analyzed by SDS-PAGE.

TFIIA was expressed and purified using an established protocol [41]. All proteins were concentrated and stored at -80°C . All constructs are listed in Appendix Table S3.

Protein crystallization and structure determination

Native Kap114p crystals were obtained using a hanging drop vapor diffusion method with a 17.6 mg/ml protein concentration at 20°C by mixing 1 μl protein with 1 μl reservoir solution of 0.43 M citric acid, 0.057 M bis-tris propane (pH 5.8), 17% PEG3350, 0.01 M

ethylenediaminetetraacetic acid disodium salt dihydrate, and 3% v/v ethanol. Selenium-labeled crystals were grown in 0.044 M citric acid, 0.056 M bis-tris propane (pH 5.6), 15% PEG3350, and 0.5% w/v polyvinylpyrrolidone. Crystals appeared in about one week. Crystals were hexagonal (space group $P3_12_1$), with one molecule per asymmetric unit. Data were collected at beamline 13B, 13C, and 05A in the National Synchrotron Radiation Research Centre (Taiwan). X-ray intensities were processed using HKL2000 [54]. Phase determination was carried out using data collected from seleno-L-methionine-labeled crystals at selenium peak and inflection wavelengths using PHENIX [55]. The initial model was built into the electron density map and refined using PHENIX and Coot [55,56]. The final structure was refined to a resolution of 2.5 Å with an R-factor of 20.6% (Rfree 25.5%), and there were no outliers in the Ramachandran plot.

Pull-down assays

GST-tagged γ TBP (61–240) (1 μ M) was preincubated with MagnetGST™ Glutathione Particles (Promega) in binding buffer containing 20 mM HEPES (pH 7.4), 150 mM NaCl, and 3 mM DTT, on ice for 30 min, before adding 1 μ M of Kap114p, Kap114p (Δ 347–371), or Kap114p (Δ 899–956) for incubation for another 30 min. The reactions were washed three times using binding buffer and then eluted by 50 mM glutathione. The eluted samples were analyzed by SDS–PAGE. His-tagged RanQ69L (4 μ M) was preincubated on ice with MagnetHis™ Ni-Particles (Promega) in phosphate-binding buffer with 150 mM NaCl and 3 mM β -mercaptoethanol for 30 min. We added 1 μ M of Kap95p, Kap114p, or Kap121p to the reaction before incubating it for another 30 min on ice. The reactions were washed three times and eluted by buffer containing 250 mM imidazole, and analyzed by SDS–PAGE. For competitive binding analysis, Kap114p (0.5 μ M), GST-tagged γ TBP (61–240) (2 μ M), and His-tagged RanQ69L (4 μ M) were preincubated and pulled down by MagnetGST™ Glutathione Particles (Promega).

Small angle X-ray scattering

Purified Kap114, Kap114-RanQ60L, and Kap114p- γ TBP complexes were diluted to 5 mg/ml in buffer [20 mM HEPES (pH 7.4), 150 mM NaCl, 3 mM DTT] before being subjected to SAXS analysis. Data were collected at the SAXS beamline 23A in the Taiwan Light Source of the National Synchrotron Radiation Research Centre [57,58]. The experimental setup consists of a High Pressure Liquid Chromatography (HPLC, Agilent chromatographic system 1,260 series) system equipped with an Agilent silica-based column of pore size 300 Å, followed downstream by a SAXS sample capillary. An X-ray beam with wavelength of 0.8266 Å was used for data collection. Selected frames were merged and analyzed for initial R_g estimation by the PRIMUS program, and the $P(r)$ distance distribution was determined by the GNOM program, both from the ATSAS package [59]. Low-resolution *ab initio* envelopes were calculated using DAMMIF and GASBOR. DAMAVER was then used to generate an average model, and the crystal structures were fitted into the envelope by SUPCOMB. SAXS modeling of the Kap114p-Ran and Kap114p- γ TBP complexes was performed using FoXSDock [60,61].

Isothermal titration calorimetry

Binding affinities between γ TBP and Kap114p, Kap114p (Δ 347–371), Kap114p (Δ 899–956), Kap95p, and Kap121p were measured by ITC (MicroCal iTC200). All proteins (500 μ M of γ TBP and 50 μ M of Kap- β s, i.e., Kap114p WT/mutants, Kap95p, and Kap121p) were dialyzed against ITC buffer [20 mM HEPES (pH 7.4), 150 mM NaCl, 1 mM β -mercaptoethanol]. Different Kap proteins were stored in the sample cell, and γ TBP was injected into the cell by syringe. ITC was performed at 25°C. The experimental data were fitted to theoretical titration curves with the software supplied by MicroCal (ORIGIN).

Electrophoretic mobility shift assay

Electrophoretic mobility shift assay (EMSA) was performed using purified recombinant γ TBP, TFIIA, and Kap114p. We used synthesized FAM (fluorescein amidite) 5'-labeled TATA-box double-stranded DNA (TGTATGTATATAAAAC). Samples were analyzed by 4.5% polyacrylamide gels [4.5% acrylamide from a 29%:1% acrylamide:bisacrylamide stock, 25 mM Tris–HCl (pH 8.3), 190 mM glycine, 10 mM EDTA] using TGE running buffer [25 mM Tris–HCl (pH 8.3), 190 mM glycine, 10 mM EDTA]. Gels were pre-run at 100 V at 4°C for 1 h before sample loading. Proteins and DNA were incubated on ice at 60 min in 20 mM HEPES (pH 8.3), 100 mM NaCl, 3 mM MgCl₂, 1 mM DTT, 0.1 mg/ml bovine serum albumin (BSA), and 4% glycerol.

Analytic ultracentrifugation

Sedimentation velocity analyses were conducted at 262,080 g at 20°C with a Beckman Coulter ProteomeLab XL-I AUC system equipped with absorbance optics. Purified protein samples of γ TBP, Kap114p, and Kap114p- γ TBP were diluted to final concentrations of 1.1, 0.86, and 1.47 mg/ml, respectively. The dilution was performed using 20 mM HEPES (pH 7.4), 150 mM NaCl, and 1 mM DTT prior to analysis. Standard 12 mm aluminum double-sector centerpieces were filled with the protein solution, whereas blank buffer was used in the reference cell. Before each run, cells were thermally equilibrated for at least 1 h in the four-hole (AnTi60) rotor of the instrument. Quartz windows were used with absorbance optics (OD 280 nm) in continuous mode without averaging. No time interval was set between scans. For sedimentation equilibrium experiments, the Kap114p- γ TBP complex was diluted to 0.84 mg/ml and analyzed at 3,244 g, 4,648 g, and 14,598 g using a four-hole AnTi60 rotor at 20°C. Data were analyzed with a $c(s)$ distribution of Lamm equation solutions calculated by the program SEDFIT (www.analyticalultracentrifugation.com), assuming the regularization parameter P to be 0.95 (high-confidence level). The weighted average sedimentation coefficient (S) was obtained by integration over the range of each peak. All S values were corrected for the viscosity and density of water at 20°C.

Yeast strain construction

KAP114 (including the upstream 500 base pairs (bp) and downstream 100 bp) was cloned into the vector pRS426. We deleted *KAP114* from the YTK12029 strains [24] by replacing it with a gene

encoding LEU2. We amplified the LEU2 sequence from pFA6a LEU2 template using the forward primer AAAATCTTGAACGTAATTGTAACACTATCAACACATTAACCGGATCCCCGGGTTAATTAA and the reverse primer CTACTTTACATCTGATATCTCCACGGCTTATGTATATAAGGAATTCGAGCTCGTTTAAAC. The PCR product was transformed into both strains. Genomic DNA of colonies grown on the selective medium was isolated and verified by PCR. The *KAP114* knockout strain SC1005 was transformed with pRS426 as a control or pRS426 carrying wild-type *KAP114*, *KAP114* ($\Delta 347-371$), and *KAP114* ($\Delta 899-956$) (SC1008-SC1010). To generate the *KAP114* knockout strain carrying GFP-labeled yTBP, we deleted the endogenous *KAP114* from the YER148W strain by replacing it with a gene encoding LEU2. All yeast strains used in this study are listed in Appendix Table S2.

Yeast spot-based assay

Yeast strains were grown at 30°C in YPD medium, or in minimal medium (-Ura, -His, -Leu2). For dilution spot assays, yeast samples grown to logarithmic phase were initially diluted to the same OD. Subsequently, a series of fivefold dilutions was generated, and then, 10 μ l of each sample was spotted onto selective medium and incubated at the indicated temperatures. To examine yeast growth under stress conditions, yeast spots were performed in YPD medium to which was added 1 M sorbitol, 1.5 M NaCl, 0.5% acetic acid, or 0.01% MMS and incubated at the indicated temperatures.

RNA-seq and bioinformatics analyses

Yeast strains YTK12029 and SC1005 were grown in YPD medium with or without 1.5 M NaCl at 30°C to reach logarithmic phase. Total RNA was extracted using a RNeasy Mini Kit (QIAGEN). RNA quality control and quantification were performed using an Agilent 2100 Bioanalyzer. The mRNA sequencing libraries were prepared using a TruSeq Stranded mRNA kit (Illumina), and 75 cycle single-read sequencing was performed using the 500 High-output v2 sequencing kit on an Illumina NextSeq500 instrument. Adaptor sequences were removed, and raw sequence quality was examined using FastQC software. Bioinformatics analysis was performed using two systems. The first analysis was conducted in CLC Genomics Workbench (v.11.0.1, <http://www.clcbio.com>). Raw sequencing reads were trimmed of low-quality sequences (Phred quality score of < 20) and of sequences with length < 25 base pairs. Sequencing reads were mapped to the yeast S288C genome assembly (*Saccharomyces cerevisiae*.R64-1-1.82) from Ensembl with the following parameters: mismatches cost = 2, insertion cost = 3, deletion cost = 3, minimum fraction length = 0.9, minimum fraction similarity = 0.9, and maximum hits per read = 5. A generalized linear model (GLM) and Wald test were then used to analyze differential expression of genes and their statistical significance. The second system employed Hisat2 for sequence mapping with default settings, using the feature Counts for counting reads, and classic edgeR and Fisher's exact test to assess differential expression and for statistical analysis. To analyze results from both systems, we first set a false discovery rate (FDR) of $P < 0.05$ to select significantly altered genes. Then, we stipulated a fold change > 1.5 and < -1.5 for

down- and up-regulated genes, respectively. To remove genes with background expression levels, average transcripts per kilobase million (TPM) were carried out for data normalization and had set to be > 10. Principal component analysis (PCA) was also used to reveal relationships among triplicate samples. To generate the heat map, we grouped genes into clusters on the basis of Euclidean distance by using Multiple Experiment Viewer (MeV 4.9.0).

RT-qPCR

Yeast strains YTK12029 and SC1005 were grown in YPD and minimal medium with or without 1.5 M NaCl at 30°C to reach logarithmic phase. Total RNAs were extracted using a RNeasy Mini Kit (QIAGEN) and were reverse-transcribed to cDNA using RevertAid Reverse Transcriptase (ThermoScientific) in a 20 μ l reaction system. RT-PCR was performed using Fast SYBRTM Green Master Mix (ThermoScientific), and relative expression levels were normalized to the level of actin. RT-PCR was carried out using a QuantStudioTM 12K Flex Real-Time PCR System (ThermoScientific), and the quantitative RT-PCR data were analyzed by the comparative C_t method ($\Delta\Delta C_t$).

Yeast whole-cell extract isolation

Yeast cells were grown in the minimal medium with or without 1.5 M NaCl to reach logarithmic phase. The cells were harvested by centrifugation and washed with 1 \times PBS buffer. After centrifugation, cells were resuspended in 300 μ l lysis buffer (50 mM Tris at pH 7.5, 150 mM NaCl, 1 mM EDTA, 10% glycerol, 0.05% Triton X-100, 1 mM PMSF, and 1 mM DTT). Glass beads (BioSpec) were added, and the mixture was vortexed with a Mini-BeadBeater (BioSpec) for 5 cycles (45-s vortex, cooling on ice for 1 min between each cycle) in the cold room. Whole-cell extracts were collected after centrifugation and analyzed by Western blot analysis.

Visualization of yTBP-GFP in living cells

Yeast strains SC1007-10- and YER148W-GFP-expressing yTBP-GFP were grown to logarithmic phase. An AxioImager-Z1 fluorescence microscope (Zeiss) equipped with a Cool SNAP HQ2 camera (Photometrics) and a 100 \times DIC objective were used to observe the yeast cells. Images were captured by using Zen 2.5 blue edition software (Zeiss).

Immunoblotting

Yeast strains YER148W-GFP-expressing yTBP-GFP were grown in YPD medium with or without 1.5 M NaCl at 30°C to reach logarithmic phase. The nuclei were extracted using a Yeast Nuclei Isolation Kit (Abcam/ab206997), and quality of nuclei was checked under a fluorescence microscope. Yeast nuclear proteins were analyzed by 10% gradient SDS-PAGE, following by immunoblotting with PCNA (GeneTex/GTX64144), Ran (GeneTex/GTX80345), and anti-GFP antibody (Abcam/ab183734). Yeast whole-cell extracts contain the Kap114 FLAG-tagged proteins were analyzed using anti-DDDDK (GeneTex/GTX115043) and anti-tubulin antibody (Abcam/ab6160).

ChIP-qPCR

Yeast strains YER148W-GFP- and SC1007-expressing γ TBP-GFP were grown in YPD medium with or without 1.5 M NaCl at 30°C to reach the logarithmic phase ($OD_{600} = 0.8$). Cells were cross-linked with 1% formaldehyde (Sigma) for 15 min and subsequently quenched with 125 mM glycine for 5 min at room temperature. Fixed cells were washed with ice-cold ST Buffer (10 mM Tris-HCl, pH 7.5, 100 mM NaCl) and lysed in FA Lysis Buffer (50 mM HEPES-KOH, pH 7.5, 150 mM NaCl, 2 mM EDTA, 1% Triton, 0.1% sodium deoxycholate, and protease inhibitor cocktail) with a bead beater (MP Biomedicals). The chromatin was pelleted by centrifugation and fragmented in FA lysis buffer supplemented with 0.1% SDS with a Bioruptor (Diagenode). Chromatin immunoprecipitation was performed with 50 ml culture-equivalent of chromatin and anti-GFP antibody (Abcam, CHIP grade (ab290)). The ChIPed DNA was quantified with SYBR green master mix in a StepOnePlus™ Real-Time PCR System (Applied Biosystems). Normalized C_t (ΔC_t) values were calculated by subtracting the C_t value of the promoter of each gene from the C_t value of a reference region (1 kb downstream of the ACT core promoter) ($\Delta C_t = C_{t_{ref}} - C_{t_{promoter}}$). Data are presented as fold change for each gene by comparing the ΔC_t value of salt-treated to untreated samples. Gene-specific primers are listed in Appendix Table S2.

Data availability

Coordinates and structure-factor files have been deposited in the Protein Data Bank, with accession code 6AHO (<https://www.rcsb.org/structure/6AHO>). The RNA-seq data from this study have been submitted to the NCBI Gene Expression Omnibus (Accession number GSE127178; <https://www.ncbi.nlm.nih.gov/geo/query/acc.cgi?acc=GSE127178>).

Expanded View for this article is available online.

Acknowledgements

We appreciate the technical services provided by the “Synchrotron Radiation Protein Crystallography Facility of the National Core Facility Program for Biotechnology, Ministry of Science and Technology” and the “National Synchrotron Radiation Research Center”, a national user facility supported by the Ministry of Science and Technology of Taiwan, ROC. We also thank John O'Brien for manuscript editing and the IMB Bioinformatics, Genomics, and Imaging cores for technical assistance. We acknowledge the use of the ITC and AUC in the Biophysics Core Facility, funded by Academia Sinica Core Facility and Innovative Instrument Project (AS-CFII108-111). We thank Tetsuro Kokubo for yeast strains. We also thank Toshiya Senda for bacterial expression construct of TFIIA. K.-C.H. acknowledges support from the Ministry of Science and Technology (MOST-106-2311-B-001-038-MY3) and Academia Sinica (AS-CDA-106-LO2). W.-Y.C. acknowledges support from the Ministry of Science and Technology (MOST-107-2320-B-010-024-MY3).

Author contributions

C-CL, C-CC, and GRA performed biochemical experiments. C-CL prepared samples for transcriptome analyses. C-CL and SS carried out yeast-based experiments. C-CL and K-CH determined crystal structures. W-CP and W-YC performed ChIP-qPCR experiments. All authors analyzed the data, discussed

the results, and helped write the manuscript. K-CH directed the project and prepared the manuscript.

Conflict of interest

The authors declare that they have no conflict of interest.

References

- Causton HC, Ren B, Koh SS, Harbison CT, Kanin E, Jennings EG, Lee TI, True HL, Lander ES, Young RA (2001) Remodeling of yeast genome expression in response to environmental changes. *Mol Biol Cell* 12: 323–337
- Gasch AP, Spellman PT, Kao CM, Carmel-Harel O, Eisen MB, Storz G, Botstein D, Brown PO (2000) Genomic expression programs in the response of yeast cells to environmental changes. *Mol Biol Cell* 11: 4241–4257
- Bhuiyan T, Timmers HTM (2019) Promoter recognition: putting TFIID on the spot. *Trends Cell Biol* 29: 752–763
- Roeder RG (2019) 50+ years of eukaryotic transcription: an expanding universe of factors and mechanisms. *Nat Struct Mol Biol* 26: 783–791
- Vannini A, Cramer P (2012) Conservation between the RNA polymerase I, II, and III transcription initiation machineries. *Mol Cell* 45: 439–446
- Sainsbury S, Bernecky C, Cramer P (2015) Structural basis of transcription initiation by RNA polymerase II. *Nat Rev Mol Cell Biol* 16: 129–143
- Irvin JD, Pugh BF (2006) Genome-wide transcriptional dependence on TAF1 functional domains. *J Biol Chem* 281: 6404–6412
- Gumbs OH, Campbell AM, Weil PA (2003) High-affinity DNA binding by a Mot1p-TBP complex: implications for TAF-independent transcription. *EMBO J* 22: 3131–3141
- Pereira LA, Klejman MP, Timmers HT (2003) Roles for BTAf1 and Mot1p in dynamics of TATA-binding protein and regulation of RNA polymerase II transcription. *Gene* 315: 1–13
- Chitikila C, Huisinga KL, Irvin JD, Basehoar AD, Pugh BF (2002) Interplay of TBP inhibitors in global transcriptional control. *Mol Cell* 10: 871–882
- Geisberg JV, Struhl K (2004) Cellular stress alters the transcriptional properties of promoter-bound Mot1-TBP complexes. *Mol Cell* 14: 479–489
- Auble DT, Hansen KE, Mueller CG, Lane WS, Thorner J, Hahn S (1994) Mot1, a global repressor of RNA polymerase II transcription, inhibits TBP binding to DNA by an ATP-dependent mechanism. *Genes Dev* 8: 1920–1934
- Zentner GE, Henikoff S (2013) Mot1 redistributes TBP from TATA-containing to TATA-less promoters. *Mol Cell Biol* 33: 4996–5004
- Hsu JY, Juven-Gershon T, Marr MT II, Wright KJ, Tjian R, Kadonaga JT (2008) TBP, Mot1, and NC2 establish a regulatory circuit that controls DPE-dependent versus TATA-dependent transcription. *Genes Dev* 22: 2353–2358
- Tora L, Timmers HT (2010) The TATA box regulates TATA-binding protein (TBP) dynamics *in vivo*. *Trends Biochem Sci* 35: 309–314
- Imbalzano AN, Zaret KS, Kingston RE (1994) Transcription factor (TF) IIB and TFIIA can independently increase the affinity of the TATA-binding protein for DNA. *J Biol Chem* 269: 8280–8286
- Tan S, Hunziker Y, Sargent DF, Richmond TJ (1996) Crystal structure of a yeast TFIIA/TBP/DNA complex. *Nature* 381: 127–151

18. Weideman CA, Netter RC, Benjamin LR, McAllister JJ, Schmiedekamp LA, Coleman RA, Pugh BF (1997) Dynamic interplay of TFIIA, TBP and TATA DNA. *J Mol Biol* 271: 61–75
19. Yokomori K, Zeidler MP, Chen JL, Verrijzer CP, Mlodzik M, Tjian R (1994) Drosophila TFIIA directs cooperative DNA binding with TBP and mediates transcriptional activation. *Genes Dev* 8: 2313–2323
20. Auble DT, Hahn S (1993) An ATP-dependent inhibitor of TBP binding to DNA. *Genes Dev* 7: 844–856
21. Kamada K, Shu F, Chen H, Malik S, Stelzer G, Roeder RG, Meisterernst M, Burley SK (2001) Crystal structure of negative cofactor 2 recognizing the TBP-DNA transcription complex. *Cell* 106: 71–81
22. Bagby S, Mal TK, Liu D, Raddatz E, Nakatani Y, Ikura M (2000) TFIIA-TAF regulatory interplay: NMR evidence for overlapping binding sites on TBP. *FEBS Lett* 468: 149–154
23. Liu D, Ishima R, Tong KI, Bagby S, Kokubo T, Muhandiram DR, Kay LE, Nakatani Y, Ikura M (1998) Solution structure of a TBP-TAF(II)230 complex: protein mimicry of the minor groove surface of the TATA box unwound by TBP. *Cell* 94: 573–583
24. Anandapadamanaban M, Andresen C, Helander S, Ohyama Y, Siponen MI, Lundstrom P, Kokubo T, Ikura M, Moche M, Sunnerhagen M (2013) High-resolution structure of TBP with TAF1 reveals anchoring patterns in transcriptional regulation. *Nat Struct Mol Biol* 20: 1008–1014
25. Gupta K, Watson AA, Baptista T, Scheer E, Chambers AL, Koehler C, Zou J, Obong-Ebong I, Kandiah E, Temblador A et al (2017) Architecture of TAF11/TAF13/TBP complex suggests novel regulation properties of general transcription factor TFIID. *Elife* 6: e30395
26. Coleman RA, Taggart AK, Benjamin LR, Pugh BF (1995) Dimerization of the TATA binding protein. *J Biol Chem* 270: 13842–13849
27. Chasman DI, Flaherty KM, Sharp PA, Kornberg RD (1993) Crystal structure of yeast TATA-binding protein and model for interaction with DNA. *Proc Natl Acad Sci USA* 90: 8174–8178
28. Nikolov DB, Hu SH, Lin J, Gasch A, Hoffmann A, Horikoshi M, Chua NH, Roeder RG, Burley SK (1992) Crystal structure of TFIID TATA-box binding protein. *Nature* 360: 40–46
29. Morehouse H, Buratowski RM, Silver PA, Buratowski S (1999) The importin/karyopherin Kap114 mediates the nuclear import of TATA-binding protein. *Proc Natl Acad Sci USA* 96: 12542–12547
30. Pemberton LF, Rosenblum JS, Blobel G (1999) Nuclear import of the TATA-binding protein: mediation by the karyopherin Kap114p and a possible mechanism for intranuclear targeting. *J Cell Biol* 145: 1407–1417
31. Matsuura Y, Stewart M (2004) Structural basis for the assembly of a nuclear export complex. *Nature* 432: 872–877
32. Kutay U, Bischoff FR, Kostka S, Kraft R, Gorlich D (1997) Export of importin alpha from the nucleus is mediated by a specific nuclear transport factor. *Cell* 90: 1061–1071
33. Matsuura Y (2016) Mechanistic insights from structural analyses of Ran-GTPase-driven nuclear export of proteins and RNAs. *J Mol Biol* 428: 2025–2039
34. Greiner M, Caesar S, Schlenstedt G (2004) The histones H2A/H2B and H3/H4 are imported into the yeast nucleus by different mechanisms. *Eur J Cell Biol* 83: 511–520
35. Mosammaparast N, Ewart CS, Pemberton LF (2002) A role for nucleosome assembly protein 1 in the nuclear transport of histones H2A and H2B. *EMBO J* 21: 6527–6538
36. Fox AM, Ciziene D, McLaughlin SH, Stewart M (2011) Electrostatic interactions involving the extreme C terminus of nuclear export factor CRM1 modulate its affinity for cargo. *J Biol Chem* 286: 29325–29335
37. Christie M, Chang CW, Rona G, Smith KM, Stewart AG, Takeda AA, Fontes MR, Stewart M, Vertessy BG, Forwood JK et al (2016) Structural biology and regulation of protein import into the nucleus. *J Mol Biol* 428: 2060–2090
38. Conti E, Izaurralde E (2001) Nucleocytoplasmic transport enters the atomic age. *Curr Opin Cell Biol* 13: 310–319
39. Chook YM, Blobel G (2001) Karyopherins and nuclear import. *Curr Opin Struct Biol* 11: 703–715
40. Mal TK, Masutomi Y, Zheng L, Nakata Y, Ohta H, Nakatani Y, Kokubo T, Ikura M (2004) Structural and functional characterization on the interaction of yeast TFIID subunit TAF1 with TATA-binding protein. *J Mol Biol* 339: 681–693
41. Adachi N, Aizawa K, Kratzer Y, Saijo S, Shimizu N, Senda T (2017) Improved method for soluble expression and rapid purification of yeast TFIIA. *Protein Expr Purif* 133: 50–56
42. Veis J, Klug H, Koranda M, Ammerer G (2007) Activation of the G2/M-specific gene CLB2 requires multiple cell cycle signals. *Mol Cell Biol* 27: 8364–8373
43. Miyamoto Y, Saiwaki T, Yamashita J, Yasuda Y, Kotera I, Shibata S, Shigetani M, Hiraoka Y, Haraguchi T, Yoneda Y (2004) Cellular stresses induce the nuclear accumulation of importin alpha and cause a conventional nuclear import block. *J Cell Biol* 165: 617–623
44. O'Reilly AJ, Dacks JB, Field MC (2011) Evolution of the karyopherin-beta family of nucleocytoplasmic transport factors; ancient origins and continued specialization. *PLoS ONE* 6: e19308
45. Chou CC, Wang AH (2015) Structural D/E-rich repeats play multiple roles especially in gene regulation through DNA/RNA mimicry. *Mol BioSyst* 11: 2144–2151
46. Lieb JD, Liu X, Botstein D, Brown PO (2001) Promoter-specific binding of Rap1 revealed by genome-wide maps of protein-DNA association. *Nat Genet* 28: 327–334
47. Lee TI, Rinaldi NJ, Robert F, Odom DT, Bar-Joseph Z, Gerber GK, Hannett NM, Harbison CT, Thompson CM, Simon I et al (2002) Transcriptional regulatory networks in *Saccharomyces cerevisiae*. *Science* 298: 799–804
48. Warner JR (1999) The economics of ribosome biosynthesis in yeast. *Trends Biochem Sci* 24: 437–440
49. Martin DE, Souillard A, Hall MN (2004) TOR regulates ribosomal protein gene expression via PKA and the Forkhead transcription factor FHL1. *Cell* 119: 969–979
50. Glass CK, Saijo K (2010) Nuclear receptor transrepression pathways that regulate inflammation in macrophages and T cells. *Nat Rev Immunol* 10: 365–376
51. Rothenbusch U, Sawatzki M, Chang Y, Caesar S, Schlenstedt G (2012) Sumoylation regulates Kap114-mediated nuclear transport. *EMBO J* 31: 2461–2472
52. Padavannil A, Sarkar P, Kim SJ, Cagatay T, Jiou J, Brautigam CA, Tomchick DR, Sali A, D'Arcy S, Chook YM (2019) Importin-9 wraps around the H2A-H2B core to act as nuclear importer and histone chaperone. *Elife* 8: e43630
53. Mosammaparast N, Del Rosario BC, Pemberton LF (2005) Modulation of histone deposition by the karyopherin kap114. *Mol Cell Biol* 25: 1764–1778
54. Otwinowski Z, Minor W (1997) Processing of X-ray diffraction data collected in oscillation mode. *Methods Enzymol* 276: 307–326
55. Adams PD, Afonine PV, Bunkoczi G, Chen VB, Davis IW, Echols N, Headd JJ, Hung LW, Kapral GJ, Grosse-Kunstleve RW et al (2010) PHENIX: a

- comprehensive Python-based system for macromolecular structure solution. *Acta Crystallogr D Biol Crystallogr* 66: 213–221
56. Emsley P, Cowtan K (2004) Coot: model-building tools for molecular graphics. *Acta Crystallogr D Biol Crystallogr* 60: 2126–2132
 57. Yeh YQ, Liao KF, Shih O, Shiu YJ, Wu WR, Su CJ, Lin PC, Jeng US (2017) Probing the acid-induced packing structure changes of the molten globule domains of a protein near equilibrium unfolding. *J Phys Chem Lett* 8: 470–477
 58. Shih O, Yeh YQ, Liao KF, Su CJ, Wu PH, Heenan RK, Yu TY, Jeng US (2018) Membrane charging and swelling upon calcium adsorption as revealed by phospholipid nanodiscs. *J Phys Chem Lett* 9: 4287–4293
 59. Franke D, Petoukhov MV, Konarev PV, Panjkovich A, Tuukkanen A, Mertens HDT, Kikhney AG, Hajizadeh NR, Franklin JM, Jeffries CM et al (2017) ATSAS 2.8: a comprehensive data analysis suite for small-angle scattering from macromolecular solutions. *J Appl Crystallogr* 50: 1212–1225
 60. Schneidman-Duhovny D, Hammel M, Sali A (2011) Macromolecular docking restrained by a small angle X-ray scattering profile. *J Struct Biol* 173: 461–471
 61. Schneidman-Duhovny D, Hammel M, Tainer JA, Sali A (2016) FoXS, FoXS-Dock and MultiFoXS: single-state and multi-state structural modeling of proteins and their complexes based on SAXS profiles. *Nucleic Acids Res* 44: W424–W429